Entanglement Growth from Entangled States: A Unified Perspective on Entanglement Generation and Transport

Chun-Yue Zhang,[1,2] Zi-Xiang Li,[1,2,*] and Shi-Xin Zhang[1,†]

[1] *Beijing National Laboratory for Condensed Matter Physics & Institute of Physics, Chinese Academy of Sciences, Beijing 100190, China*

[2] *University of Chinese Academy of Sciences, Beijing 100049, China*

(Dated: October 10, 2025)

Studies of entanglement dynamics in quantum many-body systems have focused largely on initial product states. Here, we investigate the far richer dynamics from initial entangled states, uncovering universal patterns across diverse systems ranging from many-body localization (MBL) to random quantum circuits. Our central finding is that the growth of entanglement entropy can exhibit a non-monotonic dependence on the initial entanglement in many non-ergodic systems, peaking for moderately entangled initial states. To understand this phenomenon, we introduce a conceptual framework that decomposes entanglement growth into two mechanisms: "build" and "move". The "build" mechanism creates new entanglement, while the "move" mechanism redistributes pre-existing entanglement throughout the system. We model a pure "move" dynamics with a random SWAP circuit, showing it uniformly distributes entanglement across all bipartitions. We find that MBL dynamics are "move-dominated", which naturally explains the observed non-monotonicity of the entanglement growth. This "build-move" framework offers a unified perspective for classifying diverse physical dynamics, deepening our understanding of entanglement propagation and information processing in quantum many-body systems.

Introduction.—Entanglement is a cornerstone of modern physics [1–4], specifically, the entanglement entropy (EE) has emerged as a key diagnostic for non-equilibrium quantum dynamics [4–9]. The standard approach investigates the time evolution of entanglement from an initial product state, revealing a rich landscape of dynamical behaviors. In thermalized systems and generic random quantum circuits (RQCs), entanglement grows rapidly, often linearly in time [10–25]. In contrast, many-body localized (MBL) systems [26–62] exhibit a much slower, logarithmic growth [63–69], while integrable systems saturate to non-thermal values [70–74] and non-interacting Anderson localized (AL) systems show severely suppressed entanglement growth [75–87]. However, this fruitful paradigm inherently conflates two distinct aspects of entanglement dynamics: the initial generation of entangled resources, and the subsequent transport of this entanglement. The observed half-chain entanglement entropy (HCEE) growth is thus always a composite effect, leaving the underlying pattern of entanglement propagation obscured.

To deconstruct this process and isolate the intrinsic entanglement handling capabilities of a given system, we shift the paradigm to study the evolution of initial states that already possess volume-law entanglement, which we term partially thermalized states. These states are thus prepared to contain a rich, pre-existing reservoir of entanglement, providing a non-trivial substrate for the subsequent dynamics. This paradigm shift allows us to move from the question "how fast is entanglement created?" to a more profound one: "how does a system's inherent dynamics process and redistribute pre-existing entanglement?". This setup facilitates deep probing into the intricate interplay between a system's fundamental character and an existing, complex entanglement structure.

In this Letter, we address these questions and uncover a remarkable phenomenon: in MBL dynamics, the HCEE growth exhibits a non-monotonic behavior with its initial value, profoundly differing from thermalized systems (see Fig. 1(d)). To rationalize the observed behaviors, we introduce a novel conceptual framework that decomposes HCEE growth into two primary mechanisms: "build" for creating new entanglement and "move" for redistributing pre-existing entanglement, as schematically shown in Fig. 1(a,b). We demonstrate that this framework not only successfully explains our results by identifying MBL as a "move-dominated" dynamics, but also provides a unified perspective for classifying diverse quantum dynamics.

Model and Methods.—We study the dynamics in a one-dimensional spin-1/2 chain of even length L using exact diagonalization. The central quantity of interest is the HCEE measured in bits: $S = -\operatorname{Tr}(\hat{\rho}_{\rm HC}\log_2\hat{\rho}_{\rm HC})$, defined as the von Neumann entropy of the first $L/2$ spins whose reduced density operator is $\hat{\rho}_{\rm HC}$. The various physical processes in our study, from initial state preparation to subsequent dynamics, are mainly based on the one-dimensional disordered XXZ Hamiltonian with open boundary conditions:

$$\hat{H} = \sum_{i=1}^{L-1}\left(\hat{S}_i^x\hat{S}_{i+1}^x + \hat{S}_i^y\hat{S}_{i+1}^y + J_z\hat{S}_i^z\hat{S}_{i+1}^z\right) + \sum_{i=1}^{L} h_i\hat{S}_i^z. \tag{1}$$

Here, $\hat{S}_i^\alpha$ $(\alpha = x, y, z)$ are the spin-1/2 operators at site i, and we set the anisotropy $J_z = 0.5$. The on-site fields h_i are independent random variables drawn uniformly

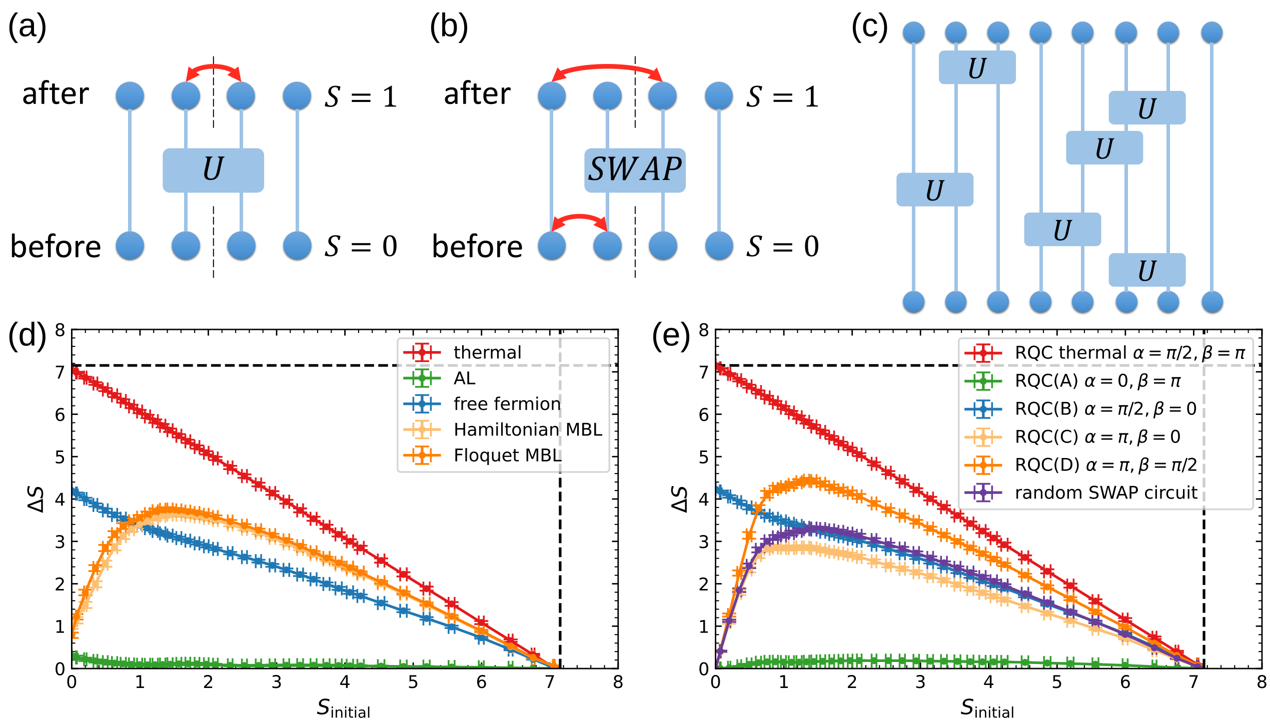

FIG. 1. The "build-move" framework and the increase of HCEE in various dynamics. (a-c) Schematic illustrations of "build" mechanism (a), "move" mechanism (b), and RQC composed of two-qubit gates U (c). Blue circles represent spins, and pairs of spins linked by red double arrows indicate Bell pairs. (d,e) Classification of dynamics based on the HCEE growth: $\Delta S = S_{\mathrm{sat}} - S_{\mathrm{initial}}$, as a function of the initial HCEE, S_{initial}. All data points are for system size $L = 16$. S_{initial} is controlled by varying the preparation time T. (d) Results for Hamiltonian-based dynamics. (e) Results for RQC-based dynamics. The two-qubit gates U are defined in Eq. (2), with parameters in various classes detailed in Table I. For the calculation details of the data in all the figures in the main text, please refer to the Supplemental Material Sec. I.

from the interval $[-W, W]$. This Hamiltonian has a $U(1)$ symmetry which conserves the total magnetization in the z-direction, $\hat{S}^z_{\mathrm{tot}} = \sum_{i=1}^{L} \hat{S}^z_i$. All our calculations are performed in the half-filling sector $\hat{S}^z_{\mathrm{tot}} = 0$. The system is in the thermal and MBL phases at $W = 0.5$ and $W = 5.0$, respectively [28] (see Supplemental Material (SM) Sec. II for details).

Our primary focus is on the evolution from initial states with varying degrees of entanglement. We prepare initial states $|\psi(T)\rangle$ by evolving a product state $|\psi_0\rangle$ under the thermal Hamiltonian $\hat{H}(W = 0.5)$ for a duration T. $|\psi_0\rangle$ is randomly chosen from the computational basis states within the half-filling sector. The evolution time T directly controls the initial entanglement and the level of thermalization as $|\psi(T)\rangle = \mathrm{e}^{-\mathrm{i}T\hat{H}(W=0.5)}|\psi_0\rangle$. Subsequently, we examine the dynamics of these prepared states under the following $U(1)$-symmetric dynamical protocols:

1. **Thermal Dynamics:** The disorder strength is $W = 0.5$ and $|\psi(T)\rangle$ evolves under the thermal Hamiltonian $\hat{H}(W = 0.5)$.

2. **Hamiltonian MBL Dynamics:** The disorder strength is quenched to $W = 5.0$ and $|\psi(T)\rangle$ evolves under the MBL Hamiltonian $\hat{H}(W = 5.0)$.

3. **Free Fermion Dynamics:** Evolution proceeds with the free fermion Hamiltonian $\hat{H}_{\mathrm{XY}}$ with $J_z = 0$ and $W = 0$ in Eq. (1).

4. **Floquet MBL Dynamics:** A periodic drive is applied using the Floquet operator $\hat{F} = \mathrm{e}^{-\mathrm{i}T_0\hat{H}_0}\mathrm{e}^{-\mathrm{i}T_1\hat{H}_{\mathrm{XY}}}$, a protocol characteristic of the Floquet MBL phase [56]. Here, $\hat{H}_0 = \sum_{i=1}^{L-1} \hat{S}^z_i \hat{S}^z_{i+1} + \sum_{i=1}^{L} h_i \hat{S}^z_i$, with disorder strength $W = 5.0$, $T_0 = 1.0$, and $T_1 = 0.4$.

5. **AL Dynamics:** The states evolve under the non-interacting AL Hamiltonian, defined by $J_z = 0$ and $W = 5.0$ in Eq. (1).

6. **RQC protocols:** We employ RQCs, which have emerged as a paradigmatic model for understanding universal aspects of many-body quantum chaos and entanglement dynamics [14, 16, 21, 22, 88–99]. Our implementation consists of circuits where at each step, a single two-qubit gate U is applied to a randomly selected adjacent pair of spins $(i, i+1)$ from the $L-1$ bonds (as shown in Fig. 1(c)). The

TABLE I. Classification of Hamiltonian-based and RQC-based dynamics on the behavior of ΔS with S_{initial}.

Hamiltonian-based dynamics	RQC-based dynamics	Tendency of ΔS with S_{initial}
thermalization	$\alpha \in (0,\pi) \cup (\pi, 2\pi)$, $\beta \in (0, 2\pi)$	monotone decreasing
MBL	$\alpha = \pi$, $\beta = \pi$ (SWAP), $\{0, 2\pi\}$ (class C), other values (class D)	first increasing, then decreasing
free fermion	$\alpha \in (0,\pi) \cup (\pi, 2\pi)$, $\beta = \{0, 2\pi\}$(class B)	monotone decreasing
AL	$\alpha = \{0, 2\pi\}$, $\beta \in (0, 2\pi)$ (class A)	almost always zero

two-qubit unitary is given by:

$$\hat{U}_{i,i+1} = \mathrm{e}^{-\mathrm{i}\alpha\left(\hat{S}_i^x \hat{S}_{i+1}^x + \hat{S}_i^y \hat{S}_{i+1}^y\right)} \mathrm{e}^{-\mathrm{i}\beta \hat{S}_i^z \hat{S}_{i+1}^z}. \tag{2}$$

Results.—To analyze the entanglement dynamics under different protocols, we first introduce a conceptual framework that decomposes the growth of HCEE into two fundamental mechanisms: "build" and "move". As shown in Fig. 1(a), the "build" mechanism creates new entanglement directly. For instance, a two-qubit unitary gate U across the central bond can generate a Bell pair from a product state, increasing the HCEE from 0 to 1. The "move" mechanism, depicted in Fig. 1(b), involves the redistribution of pre-existing entanglement. Here, an entangled pair within one subsystem is transported across the central bond, for instance, via a SWAP gate, also raising HCEE from 0 to 1. While both mechanisms often occur simultaneously in a generic interacting system, their proportional contributions are highly dependent on the specific dynamics.

To isolate the "move" mechanism, we employ the random SWAP circuit as an idealized model, which can be achieved up to a global phase by setting $\alpha = \beta = \pi$ in our RQC protocols. The key insight is that a SWAP operation merely exchanges the state of two spins. This allows us to equivalently view the action of the random SWAP circuit on a fixed bipartition as an evolution of the bipartition itself across a static state. This evolution generates transitions between the $N = \binom{L}{L/2}/2$ distinct bipartitions, establishing an ergodic Markov chain with a uniform stationary distribution (see the proof in SM Sec. III). Consequently, at sufficiently large circuit depth, every bipartition becomes equally probable. This directly implies that the steady-state HCEE under the random SWAP circuit corresponds precisely to the initial state's *bipartition-averaged entanglement entropy* (BAEE)—the entanglement entropy averaged across all N possible equal-size bipartitions: $\bar{S} = \frac{1}{N}\sum_{\mathrm{A}\in\mathcal{P}} S_{\mathrm{A}}$, where $\mathcal{P}$ is the set consisting of subsystems corresponding to all N possible bipartitions and S_{A} represents the entropy of the subsystem A on $\mathcal{P}$. The BAEE provides a more robust measure of the state's overall entanglement, invariant under SWAP dynamics which only redistributes existing entanglement. This model thus establishes a baseline for "move"-driven dynamics, enabling quantitative comparisons with more complex protocols.

For RQC protocols of $\alpha, \beta \in [0, 2\pi]$, the specific points $(\alpha, \beta) = (0,0), (0, 2\pi), (2\pi, 0)$, and $(2\pi, 2\pi)$ are trivial as the operator $\hat{U}_{i,i+1}$ can be decomposed into a tensor product of single-qubit gates. Most other values of (α, β) lead to full thermalization, as evidenced by the HCEE saturating near the Haar measure average value in the half-filling sector [100–104] which marked by dashed lines in Fig. 1(d,e), Fig. 2 and Fig. 3. Non-thermalization behavior occurs only for a set of special parameter values which can be classified into 5 categories, based on the distinct saturation values of their HCEE. Within each category, different parameter choices for (α, β) lead to dynamics with almost the same saturating HCEE value. The random SWAP circuit mentioned above is one of these 5 categories. The parameter setting for these categories is summarized in Table I.

Fig. 2(a) displays the localized dynamics for a long time starting from $|\psi(T)\rangle$, where the evolution under different non-thermal dynamics reveals distinct behaviors. For both the Hamiltonian MBL and the Floquet MBL protocols, the HCEE exhibits a characteristic slow, logarithmic growth in time. It eventually reaches a saturation value that, while significantly higher than the initial HCEE, remains well below the Haar measure average value in the half-filling sector. In sharp contrast to MBL dynamics, the evolution governed by the non-interacting AL Hamiltonian shows almost no further increase in HCEE, confirming that interactions are crucial for moving the entanglement. The dynamics under RQC protocols are presented in Fig. 2(b). RQC(A-D) display a diverse range of behaviors. RQC(A) almost fails to increase HCEE beyond the initial value. In contrast, RQC(B-D) all facilitate HCEE growth, but with distinct non-thermal steady values.

To systematically quantify the relationship between initial entanglement and subsequent entanglement growth, we analyze the total increase of HCEE, $\Delta S = S_{\text{sat}} - S_{\text{initial}}$, as a function of S_{initial}. The results, plotted in Fig. 1(d,e), reveal that the diverse dynamical protocols can be classified into three classes based on their monoticity which reflects the capability to generate and transport entanglement. This classification is not only supported by the macroscopic behavior of ΔS, but is also consistent with the microscopic action of the gate for the RQC dynamics.

Move-Dominated Dynamics. The first class of protocols is defined by a predominant "move" mechanism, whose fundamental role is to redistribute existing entanglement. As depicted in Fig. 1(d), the dynamics of MBL

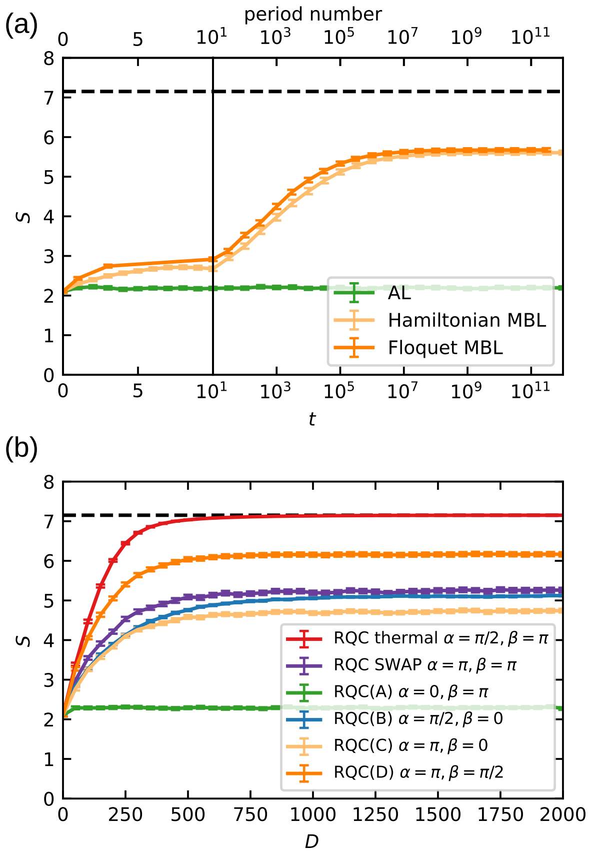

FIG. 2. Time evolution of HCEE S with initial state $|\psi(T)\rangle$ for $L = 16$ and $T = 4.5$. (a) Evolution under localized dynamics. The lower axis shows time t for AL and Hamiltonian MBL evolutions, while the upper axis shows the period number for the Floquet MBL dynamics. To visualize the dynamics across multiple timescales, the horizontal axis uses a hybrid scale of linear for the initial evolution (t, period number < 10) and logarithmic for long times. (b) Evolution under RQCs dynamics. The horizontal axis represents circuit depth. The specific (α, β) values shown in the legend are the parameters of the quantum gates selected from their respective categories.

clearly exhibit a non-monotonic dependence of ΔS on S_{initial}. This behavior, which differs significantly from that in thermal or AL dynamics, is a key finding of this Letter. For nearly product states ($S_{\text{initial}} \approx 0$), ΔS is negligible due to the minimal entanglement available for transport. It then increases to a peak for moderately entangled states before decreasing again as S_{sat} approaches the Haar measure average value. This distinct non-monotonic behavior serves as a hallmark of the "move"-dominated mechanism. Further evidence for this "move" character is found in the identical non-monotonic feature present in the random SWAP circuit dynamics, which serves as the baseline for "move"-driven dynamics. This class also encompasses RQC(C) and (D), as illustrated in Fig. 1(e). This is directly explained by their gate-level action, which functions similarly to a SWAP operator. For example, when an RQC(C) or (D) gate acts on the first two spins of the state $|\uparrow\uparrow\downarrow\rangle + |\uparrow\downarrow\uparrow\rangle$, the transformation yields $e^{-i\beta/4}|\uparrow\uparrow\downarrow\rangle - ie^{i\beta/4}|\downarrow\uparrow\uparrow\rangle$. This effectively converts entanglement from between the last two spins to between the first and third spins, thereby realizing the "move" operation at the microscopic level.

Build and Move Hybrid Dynamics. The second class of dynamics exhibits a hybrid "build-and-move" character. In conventional thermal systems, a significant ΔS emerges even from initial product states ($S_{\text{initial}} = 0$), signifying "build" mechanism that generates entanglement from scratch (Fig. 1(d)). This entanglement increase, ΔS, diminishes as S_{initial} rises. Similarly, free fermion systems also reach the equilibrium with weaker "build" capabilities due to extensive conserved quantities, resulting in a smaller ΔS. Consistent with this, RQCs with general $\alpha \in (0, \pi) \cup (\pi, 2\pi)$, including both thermal RQC and RQC(B), also show the same monotonically decreasing trend of ΔS, as shown in Fig. 1(e). The ability of these RQCs to effectively generate entanglement from product states—for instance, transforming $|\uparrow\downarrow\rangle$ into the entangled state $e^{i\beta/4}\left(\cos\frac{\alpha}{2}|\uparrow\downarrow\rangle - i\sin\frac{\alpha}{2}|\downarrow\uparrow\rangle\right)$, further corroborates the pervasive "build" mechanism within this class. Specifically, RQC(B) with $\beta = 0$ mimics free fermion dynamics. Moreover, with increasing S_{initial}, the "move" aspect for these systems also becomes a prominent contributor to the overall entanglement growth.

Entanglement-Inert Dynamics. Finally, the third class is essentially inert with respect to HCEE growth. Both AL and RQC(A) fall into this class, producing negligible ΔS across the entire range of S_{initial} (see Fig. 1(d,e)). This inert behavior stems from the lack of essential ingredients for either "build" or "move" contribution. For AL, the non-interacting and localized character of the Hamiltonian prevents entanglement from forming or spreading. For RQC(A), the underlying gate is diagonal in the computational basis, which can only affect relative phases, thereby rendering it incapable of generating or transporting entanglement.

Discussion and Conclusion.—In this Letter, we systematically investigate entanglement dynamics across diverse quantum systems, moving beyond the conventional focus on product states to explore initial states that already possess entanglement. Our central finding is a universal three-class classification of entanglement growth. Most notably, we uncover a non-monotonic dependence of HCEE increase on initial entanglement in MBL dynamics and specific RQCs—a behavior qualitatively distinct from thermal dynamics. To fundamentally account for these novel results, we introduce the "build-move" framework. This framework offers a universal lens through which to understand complex entanglement growth by classifying dynamics based on their capacity to generate new entanglement ("build") and effectively transport pre-existing entanglement ("move").

Our study yields another key insight by distinguishing between the entanglement of a single, fixed biparti-

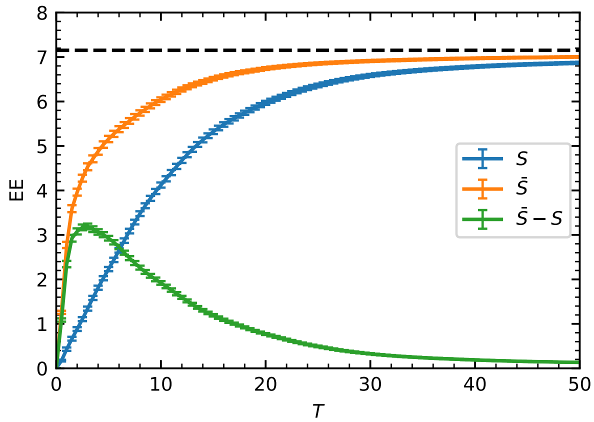

FIG. 3. Evolution of BAEE $\bar{S}$, HCEE S and their difference under $\hat{H}(W = 0.5)$ for $L = 16$, starting from the product state $|\psi_0\rangle$. The data point corresponding to the maximum value of $\bar{S} - S$ is at $T = 3.0$ with HCEE $S \approx 1.34$, roughly coinciding with the S_{initial} for the peak ΔS of move-dominated dynamics in Fig. 1(d,e).

tion (HCEE) and the overall entanglement inherent in the quantum state, which we quantify using the BAEE. Fig. 3 illustrates that, even in a generic thermalized system, the BAEE grows considerably faster than the HCEE during early dynamics. This initial divergence quantifies the rapid "build"-up of entanglement throughout the system at a local level, effectively establishing an accumulating intra-subsystem entanglement reservoir. Crucially, the existence of this reservoir explains the initial increase of ΔS with S_{initial} in move-dominated dynamics: a larger reservoir provides more entanglement potential to be "moved" across the central bond. Remarkably, the consistency is quantitative, since the peak difference between BAEE and HCEE aligns with the S_{initial} value at which ΔS peaks for MBL dynamics shown in Fig. 1(d). Given that $\bar{S} - S$ signifies the capacity for HCEE to increase through the "move" mechanism, this alignment provides compelling evidence for the "move" mechanism in MBL entanglement dynamics.

This perspective underscores the limitation of using a single bipartition's EE to fully capture a system's entanglement structure and highlights the importance of multi-partition entanglement measures, a topic of growing interest [105–107]. Our work provides a clear dynamical context for this multi-partition viewpoint. Moreover, the distinct dynamical signatures predicted by our framework present clear targets for experimental verification on near-term quantum simulation platforms, potentially opening new ways to probe and control quantum information in many-body systems.

Acknowledgement.— CYZ and ZXL are supported by Beijing Natural Science Foundation (F251001) and the National Natural Science Foundation of China (No.12347107 and No.12474146). SXZ acknowledges the support from Innovation Program for Quantum Science and Technology (2024ZD0301700) and the start-up grant at IOP-CAS.

* zixiangli@iphy.ac.cn
† shixinzhang@iphy.ac.cn

[1] O. Gühne and G. Tóth, Entanglement detection, Phys. Rep. **474**, 1 (2009).
[2] M. A. Nielsen and I. L. Chuang, Quantum computation and quantum information (Cambridge University Press, 2010).
[3] R. Horodecki, P. Horodecki, M. Horodecki, and K. Horodecki, Quantum entanglement, Rev. Mod. Phys. **81**, 865 (2009).
[4] T. Nishioka, Entanglement entropy: Holography and renormalization group, Rev. Mod. Phys. **90**, 035007 (2018).
[5] A. M. Kaufman, M. E. Tai, A. Lukin, M. Rispoli, R. Schittko, P. M. Preiss, and M. Greiner, Quantum thermalization through entanglement in an isolated many-body system, Science **353**, 794 (2016).
[6] P. Calabrese and J. Cardy, Entanglement entropy and quantum field theory, J. Stat. Mech.: Theory Exp. **2004**, P06002 (2004).
[7] C. H. Bennett, H. J. Bernstein, S. Popescu, and B. Schumacher, Concentrating partial entanglement by local operations, Phys. Rev. A **53**, 2046 (1996).
[8] T. Zhou and D. J. Luitz, Operator entanglement entropy of the time evolution operator in chaotic systems, Phys. Rev. B **95**, 094206 (2017).
[9] J. Eisert, M. Cramer, and M. B. Plenio, Colloquium: Area laws for the entanglement entropy, Rev. Mod. Phys. **82**, 277 (2010).
[10] E. Bianchi, L. Hackl, and N. Yokomizo, Linear growth of the entanglement entropy and the Kolmogorov-Sinai rate, J. High Energy Phys. **2018**, 25 (2018).
[11] Y. Han and X. Chen, Entanglement dynamics in U(1) symmetric hybrid quantum automaton circuits, Quantum **7**, 1200 (2023).
[12] M. Mezei and D. Stanford, On entanglement spreading in chaotic systems, J. High Energy Phys. **2017**, 65 (2017).
[13] J. M. Deutsch, Quantum statistical mechanics in a closed system, Phys. Rev. A **43**, 2046 (1991).
[14] T. Zhou and A. Nahum, Emergent statistical mechanics of entanglement in random unitary circuits, Phys. Rev. B **99**, 174205 (2019).
[15] M. Srednicki, Chaos and quantum thermalization, Phys. Rev. E **50**, 888 (1994).
[16] R. Oliveira, O. C. O. Dahlsten, and M. B. Plenio, Generic entanglement can be generated efficiently, Phys. Rev. Lett. **98**, 130502 (2007).
[17] A. Hamma, S. Santra, and P. Zanardi, Quantum entanglement in random physical states, Phys. Rev. Lett. **109**, 040502 (2012).
[18] H. Kim and D. A. Huse, Ballistic spreading of entanglement in a diffusive nonintegrable system, Phys. Rev. Lett. **111**, 127205 (2013).
[19] T. Rakovszky, F. Pollmann, and C. W. von Keyserlingk, Sub-ballistic growth of rényi entropies due to diffusion,

Phys. Rev. Lett. **122**, 250602 (2019).

[20] A. Nahum, J. Ruhman, S. Vijay, and J. Haah, Quantum entanglement growth under random unitary dynamics, Phys. Rev. X **7**, 031016 (2017).

[21] C. W. von Keyserlingk, T. Rakovszky, F. Pollmann, and S. L. Sondhi, Operator hydrodynamics, otocs, and entanglement growth in systems without conservation laws, Phys. Rev. X **8**, 021013 (2018).

[22] A. Nahum, S. Vijay, and J. Haah, Operator spreading in random unitary circuits, Phys. Rev. X **8**, 021014 (2018).

[23] B. Bertini, P. Kos, and T. c. v. Prosen, Entanglement spreading in a minimal model of maximal many-body quantum chaos, Phys. Rev. X **9**, 021033 (2019).

[24] M. Rigol, V. Dunjko, and M. Olshanii, Thermalization and its mechanism for generic isolated quantum systems, Nature **452**, 854 (2008).

[25] A. Russotto, F. Ares, and P. Calabrese, Symmetry breaking in chaotic many-body quantum systems at finite temperature, Phys. Rev. E **112**, L032101 (2025).

[26] D. Basko, I. Aleiner, and B. Altshuler, Metal–insulator transition in a weakly interacting many-electron system with localized single-particle states, Annals of Physics **321**, 1126 (2006).

[27] M. Žnidarič, T. c. v. Prosen, and P. Prelovšek, Many-body localization in the heisenberg xxz magnet in a random field, Phys. Rev. B **77**, 064426 (2008).

[28] A. Pal and D. A. Huse, Many-body localization phase transition, Phys. Rev. B **82**, 174411 (2010).

[29] R. Vosk and E. Altman, Many-body localization in one dimension as a dynamical renormalization group fixed point, Phys. Rev. Lett. **110**, 067204 (2013).

[30] M. Serbyn, Z. Papić, and D. A. Abanin, Local conservation laws and the structure of the many-body localized states, Phys. Rev. Lett. **111**, 127201 (2013).

[31] D. A. Huse, R. Nandkishore, and V. Oganesyan, Phenomenology of fully many-body-localized systems, Phys. Rev. B **90**, 174202 (2014).

[32] E. Altman and R. Vosk, Universal dynamics and renormalization in many-body-localized systems, Annu. Rev. Condens. Matter Phys. **6**, 383 (2015).

[33] S. Campbell, M. J. M. Power, and G. De Chiara, Dynamics and asymptotics of correlations in a many-body localized system, The European Physical Journal D **71**, 206 (2017).

[34] M. Schreiber, S. S. Hodgman, P. Bordia, H. P. Lüschen, M. H. Fischer, R. Vosk, E. Altman, U. Schneider, and I. Bloch, Observation of many-body localization of interacting fermions in a quasirandom optical lattice, Science **349**, 842 (2015).

[35] J. yoon Choi, S. Hild, J. Zeiher, P. Schauß, A. Rubio-Abadal, T. Yefsah, V. Khemani, D. A. Huse, I. Bloch, and C. Gross, Exploring the many-body localization transition in two dimensions, Science **352**, 1547 (2016).

[36] A. Lukin, M. Rispoli, R. Schittko, M. E. Tai, A. M. Kaufman, S. Choi, V. Khemani, J. Léonard, and M. Greiner, Probing entanglement in a many-body–localized system, Science **364**, 256 (2019).

[37] R. Fan, P. Zhang, H. Shen, and H. Zhai, Out-of-time-order correlation for many-body localization, Science Bulletin **62**, 707 (2017).

[38] Y. Huang, Y.-L. Zhang, and X. Chen, Out-of-time-ordered correlators in many-body localized systems, Annalen der Physik **529**, 1600318 (2017).

[39] X. Chen, T. Zhou, D. A. Huse, and E. Fradkin, Out-of-time-order correlations in many-body localized and thermal phases, Annalen der Physik **529**, 1600332 (2017).

[40] S. Liu, H.-K. Zhang, S. Yin, S.-X. Zhang, and H. Yao, Quantum mpemba effects in many-body localization systems, arXiv:2408.07750 (2024).

[41] R. Nandkishore and D. A. Huse, Many-body localization and thermalization in quantum statistical mechanics, Annu. Rev. Condens. Matter Phys. **6**, 15 (2015).

[42] R. Vasseur, S. A. Parameswaran, and J. E. Moore, Quantum revivals and many-body localization, Phys. Rev. B **91**, 140202 (2015).

[43] D. J. Luitz, N. Laflorencie, and F. Alet, Extended slow dynamical regime close to the many-body localization transition, Phys. Rev. B **93**, 060201 (2016).

[44] F. Iemini, A. Russomanno, D. Rossini, A. Scardicchio, and R. Fazio, Signatures of many-body localization in the dynamics of two-site entanglement, Phys. Rev. B **94**, 214206 (2016).

[45] T. Enss, F. Andraschko, and J. Sirker, Many-body localization in infinite chains, Phys. Rev. B **95**, 045121 (2017).

[46] R.-Q. He and Z.-Y. Lu, Characterizing many-body localization by out-of-time-ordered correlation, Phys. Rev. B **95**, 054201 (2017).

[47] K. Slagle, Z. Bi, Y.-Z. You, and C. Xu, Out-of-time-order correlation in marginal many-body localized systems, Phys. Rev. B **95**, 165136 (2017).

[48] M. Žnidarič, Entanglement in a dephasing model and many-body localization, Phys. Rev. B **97**, 214202 (2018).

[49] J. Zakrzewski and D. Delande, Spin-charge separation and many-body localization, Phys. Rev. B **98**, 014203 (2018).

[50] J. Sirker, Exploration of the existence of a distinct quasi many-body localized phase: Numerical study of a translationally invariant system in the thermodynamic limit, Phys. Rev. B **99**, 075162 (2019).

[51] J. Lee, D. Kim, and D.-H. Kim, Typical growth behavior of the out-of-time-ordered commutator in many-body localized systems, Phys. Rev. B **99**, 184202 (2019).

[52] T. Chanda, P. Sierant, and J. Zakrzewski, Time dynamics with matrix product states: Many-body localization transition of large systems revisited, Phys. Rev. B **101**, 035148 (2020).

[53] P. Sierant and J. Zakrzewski, Challenges to observation of many-body localization, Phys. Rev. B **105**, 224203 (2022).

[54] M. Serbyn, M. Knap, S. Gopalakrishnan, Z. Papić, N. Y. Yao, C. R. Laumann, D. A. Abanin, M. D. Lukin, and E. A. Demler, Interferometric probes of many-body localization, Phys. Rev. Lett. **113**, 147204 (2014).

[55] F. Andraschko, T. Enss, and J. Sirker, Purification and many-body localization in cold atomic gases, Phys. Rev. Lett. **113**, 217201 (2014).

[56] P. Ponte, Z. Papić, F. m. c. Huveneers, and D. A. Abanin, Many-body localization in periodically driven systems, Phys. Rev. Lett. **114**, 140401 (2015).

[57] S.-X. Zhang and H. Yao, Universal properties of many-body localization transitions in quasiperiodic systems, Phys. Rev. Lett. **121**, 206601 (2018).

[58] R. Vosk, D. A. Huse, and E. Altman, Theory of the many-body localization transition in one-dimensional systems, Phys. Rev. X **5**, 031032 (2015).

[59] D. A. Abanin, E. Altman, I. Bloch, and M. Serbyn, Colloquium: Many-body localization, thermalization, and entanglement, Rev. Mod. Phys. **91**, 021001 (2019).
[60] P. Sierant, M. Lewenstein, A. Scardicchio, L. Vidmar, and J. Zakrzewski, Many-body localization in the age of classical computing, Reports on Progress in Physics **88**, 026502 (2025).
[61] J. Smith, A. Lee, P. Richerme, B. Neyenhuis, P. W. Hess, P. Hauke, M. Heyl, D. A. Huse, and C. Monroe, Many-body localization in a quantum simulator with programmable random disorder, Nature Physics **12**, 907 (2016).
[62] R. Vasseur and J. E. Moore, Nonequilibrium quantum dynamics and transport: from integrability to many-body localization, J. Stat. Mech.: Theory Exp. **2016**, 064010 (2016).
[63] Y. Chen, Universal logarithmic scrambling in many body localization, arXiv:1608.02765 (2016).
[64] I. H. Kim, A. Chandran, and D. A. Abanin, Local integrals of motion and the logarithmic lightcone in many-body localized systems, arXiv:1412.3073 (2014).
[65] A. Nanduri, H. Kim, and D. A. Huse, Entanglement spreading in a many-body localized system, Phys. Rev. B **90**, 064201 (2014).
[66] D.-L. Deng, X. Li, J. H. Pixley, Y.-L. Wu, and S. Das Sarma, Logarithmic entanglement lightcone in many-body localized systems, Phys. Rev. B **95**, 024202 (2017).
[67] I. MacCormack, M. T. Tan, J. Kudler-Flam, and S. Ryu, Operator and entanglement growth in nonthermalizing systems: Many-body localization and the random singlet phase, Phys. Rev. B **104**, 214202 (2021).
[68] J. H. Bardarson, F. Pollmann, and J. E. Moore, Unbounded growth of entanglement in models of many-body localization, Phys. Rev. Lett. **109**, 017202 (2012).
[69] M. Serbyn, Z. Papić, and D. A. Abanin, Universal slow growth of entanglement in interacting strongly disordered systems, Phys. Rev. Lett. **110**, 260601 (2013).
[70] P. Calabrese and J. Cardy, Evolution of entanglement entropy in one-dimensional systems, J. Stat. Mech.: Theory Exp. **2005**, P04010 (2005).
[71] P. Calabrese and J. Cardy, Quantum quenches in extended systems, J. Stat. Mech.: Theory Exp. **2007**, P06008 (2007).
[72] K. Kawabata, T. Numasawa, and S. Ryu, Entanglement phase transition induced by the non-hermitian skin effect, Phys. Rev. X **13**, 021007 (2023).
[73] X. Feng, S. Liu, S.-X. Zhang, and S. Chen, Numerical instability of non-hermitian hamiltonian evolution, Phys. Rev. B **111**, 224310 (2025).
[74] S. Guo, S. Yin, S.-X. Zhang, and Z.-X. Li, Skin effect induced anomalous dynamics from charge-fluctuating initial states, arXiv:2504.21631 (2025).
[75] P. W. Anderson, Absence of diffusion in certain random lattices, Phys. Rev. **109**, 1492 (1958).
[76] J. Billy, V. Josse, Z. Zuo, A. Bernard, B. Hambrecht, P. Lugan, D. Clément, L. Sanchez-Palencia, P. Bouyer, and A. Aspect, Direct observation of Anderson localization of matter waves in a controlled disorder, Nature **453**, 891 (2008).
[77] B. Kramer and A. MacKinnon, Localization: theory and experiment, Reports on Progress in Physics **56**, 1469 (1993).
[78] D. Vollhardt and P. Wölfle, Diagrammatic, self-consistent treatment of the anderson localization problem in $d \leq 2$ dimensions, Phys. Rev. B **22**, 4666 (1980).
[79] T. Giamarchi and H. J. Schulz, Anderson localization and interactions in one-dimensional metals, Phys. Rev. B **37**, 325 (1988).
[80] E. Tarquini, G. Biroli, and M. Tarzia, Critical properties of the anderson localization transition and the high-dimensional limit, Phys. Rev. B **95**, 094204 (2017).
[81] I. V. Gornyi, A. D. Mirlin, and D. G. Polyakov, Interacting electrons in disordered wires: Anderson localization and low-t transport, Phys. Rev. Lett. **95**, 206603 (2005).
[82] A. De Luca, B. L. Altshuler, V. E. Kravtsov, and A. Scardicchio, Anderson localization on the bethe lattice: Nonergodicity of extended states, Phys. Rev. Lett. **113**, 046806 (2014).
[83] Y. Qing, Y.-Q. Chen, and S.-X. Zhang, Entanglement growth and information capacity in a quasiperiodic system with a single-particle mobility edge, arXiv:2506.18076 (2025).
[84] P. A. Lee and T. V. Ramakrishnan, Disordered electronic systems, Rev. Mod. Phys. **57**, 287 (1985).
[85] F. Evers and A. D. Mirlin, Anderson transitions, Rev. Mod. Phys. **80**, 1355 (2008).
[86] G. Roati, C. D'Errico, L. Fallani, M. Fattori, C. Fort, M. Zaccanti, G. Modugno, M. Modugno, and M. Inguscio, Anderson localization of a non-interacting Bose–Einstein condensate, Nature **453**, 895 (2008).
[87] K. Tikhonov and A. Mirlin, From anderson localization on random regular graphs to many-body localization, Annals of Physics **435**, 168525 (2021).
[88] Y.-Q. Chen, S. Liu, and S.-X. Zhang, Subsystem Information Capacity in Random Circuits and Hamiltonian Dynamics, Quantum **9**, 1783 (2025).
[89] M. P. Fisher, V. Khemani, A. Nahum, and S. Vijay, Random quantum circuits, Annu. Rev. Condens. Matter Phys. **14**, 335 (2023).
[90] M. Žnidarič, Exact convergence times for generation of random bipartite entanglement, Phys. Rev. A **78**, 032324 (2008).
[91] Y. Li, X. Chen, and M. P. A. Fisher, Quantum zeno effect and the many-body entanglement transition, Phys. Rev. B **98**, 205136 (2018).
[92] Y. Li, X. Chen, and M. P. A. Fisher, Measurement-driven entanglement transition in hybrid quantum circuits, Phys. Rev. B **100**, 134306 (2019).
[93] S. Liu, M.-R. Li, S.-X. Zhang, S.-K. Jian, and H. Yao, Universal kardar-parisi-zhang scaling in noisy hybrid quantum circuits, Phys. Rev. B **107**, L201113 (2023).
[94] S. Liu, M.-R. Li, S.-X. Zhang, S.-K. Jian, and H. Yao, Noise-induced phase transitions in hybrid quantum circuits, Phys. Rev. B **110**, 064323 (2024).
[95] S. Liu, M.-R. Li, S.-X. Zhang, and S.-K. Jian, Entanglement structure and information protection in noisy hybrid quantum circuits, Phys. Rev. Lett. **132**, 240402 (2024).
[96] S. Liu, H.-K. Zhang, S. Yin, and S.-X. Zhang, Symmetry restoration and quantum mpemba effect in symmetric random circuits, Phys. Rev. Lett. **133**, 140405 (2024).
[97] B. Skinner, J. Ruhman, and A. Nahum, Measurement-induced phase transitions in the dynamics of entanglement, Phys. Rev. X **9**, 031009 (2019).
[98] A. Lerose, M. Sonner, and D. A. Abanin, Influence

matrix approach to many-body floquet dynamics, Phys. Rev. X **11**, 021040 (2021).

[99] W. Wang, S. Liu, J. Li, S.-X. Zhang, and S. Yin, Driven critical dynamics in measurement-induced phase transitions, arXiv:2411.06648 (2024).

[100] R. Patil, L. Hackl, G. R. Fagan, and M. Rigol, Average pure-state entanglement entropy in spin systems with su(2) symmetry, Phys. Rev. B **108**, 245101 (2023).

[101] E. Bianchi and P. Donà, Typical entanglement entropy in the presence of a center: Page curve and its variance, Phys. Rev. D **100**, 105010 (2019).

[102] P. Vivo, M. P. Pato, and G. Oshanin, Random pure states: Quantifying bipartite entanglement beyond the linear statistics, Phys. Rev. E **93**, 052106 (2016).

[103] D. N. Page, Average entropy of a subsystem, Phys. Rev. Lett. **71**, 1291 (1993).

[104] Y. Lu, P. Shi, X.-H. Wang, J. Hu, and S.-J. Ran, Persistent ballistic entanglement spreading with optimal control in quantum spin chains, Phys. Rev. Lett. **133**, 070402 (2024).

[105] S. Singha Roy, S. N. Santalla, J. Rodríguez-Laguna, and G. Sierra, Entanglement as geometry and flow, Phys. Rev. B **101**, 195134 (2020).

[106] A. A. Akhtar and Y.-Z. You, Multiregion entanglement in locally scrambled quantum dynamics, Phys. Rev. B **102**, 134203 (2020).

[107] D. Kolisnyk, R. A. Medina, R. Vasseur, and M. Serbyn, Tensor cross interpolation of purities in quantum many-body systems, arXiv:2503.17230 (2025).

[108] V. Oganesyan and D. A. Huse, Localization of interacting fermions at high temperature, Phys. Rev. B **75**, 155111 (2007).

[109] P. Roushan, C. Neill, J. Tangpanitanon, V. M. Bastidas, A. Megrant, R. Barends, Y. Chen, Z. Chen, B. Chiaro, A. Dunsworth, A. Fowler, B. Foxen, M. Giustina, E. Jeffrey, J. Kelly, E. Lucero, J. Mutus, M. Neeley, C. Quintana, D. Sank, A. Vainsencher, J. Wenner, T. White, H. Neven, D. G. Angelakis, and J. Martinis, Spectroscopic signatures of localization with interacting photons in superconducting qubits, Science **358**, 1175 (2017).

[110] O. Bohigas, M. J. Giannoni, and C. Schmit, Characterization of chaotic quantum spectra and universality of level fluctuation laws, Phys. Rev. Lett. **52**, 1 (1984).

[111] M. L. Mehta, Random matrices (Elsevier, 2004).

[112] Y. Y. Atas, E. Bogomolny, O. Giraud, and G. Roux, Distribution of the ratio of consecutive level spacings in random matrix ensembles, Phys. Rev. Lett. **110**, 084101 (2013).

Supplemental Material for "Entanglement Growth from Entangled States: A Unified Perspective on Entanglement Generation and Transport"

CONTENTS

I. NUMERICAL DETAILS IN THE MAIN TEXT

The data presented in Fig. 1(d,e), Fig. 2 and Fig. 3 are all averaged over 72 independent runs. Each run uses one $|\psi_0\rangle$ sampled from the computational basis states within the half-filling sector and six sets of independently sampled disorders with strengths for corresponding Hamiltonian-based evolutions:

(i) one set of disorders for the thermal Hamiltonian to prepare initial state $|\psi(T)\rangle$ in Fig. 1(d,e) and Fig. 2;

(ii) four sets of disorders for thermal, Hamiltonian MBL, Floquet MBL and AL dynamics to quench $|\psi(T)\rangle$ in Fig. 1(d) and Fig. 2(a);

(iii) one set of disorders for the thermal Hamiltonian to evolve $|\psi_0\rangle$ in Fig. 3.

For the RQC protocols, the results for each run are further averaged over 5 independent circuit realizations (the bond to apply gate U at each depth).

The values of T used to generate S_{initial} of the data points in Fig. 1(d,e) are as follows:

0.0, 0.25, 0.5, 0.75, 1.0, 1.25, 1.5, 1.75, 2.0, 2.25, 2.5, 2.75, 3.0, 3.3, 3.6, 3.9, 4.2, 4.5, 5.0, 5.5, 6.0, 6.5, 7.0, 7.5, 8.0, 8.5, 9.0, 9.5, 10.0, 11.0, 12.2, 13.7, 15.7, 19.0, 24.0, 32.0, 500.0.

The values of S_{sat} in Fig. 1(d,e) are determined as follows: for thermal, Hamiltonian MBL and AL dynamics, it is the value at $t = 10^{12}$; for Floquet MBL, it is the value at the 3×10^{11}-th period; for the random SWAP circuit, it is the BAEE of the initial state $|\psi(T)\rangle$; for free fermion dynamics and RQC protocols except for random SWAP circuit, it is the average value over 100 late-time/depth snapshots (free fermion: evolution time $t = 201.0, 202.0, 203.0, \cdots, 300.0$; thermal and A-D classes of RQCs: depth $D = 1901, 1902, 1903, \cdots, 2000$).

II. THE LEVEL SPACING RATIOS DISTRIBUTION ANALYSIS FOR THERMALIZATION AND MBL

The distribution of level spacing ratios serves as a powerful probe to distinguish between thermal and MBL phases, a method rooted in random matrix theory (RMT) [28, 108–111]. We employ this diagnostic for the disordered XXZ Hamiltonian:

$$\hat{H} = \sum_{i=1}^{L-1} \left(\hat{S}_i^x \hat{S}_{i+1}^x + \hat{S}_i^y \hat{S}_{i+1}^y + J_z \hat{S}_i^z \hat{S}_{i+1}^z \right) + \sum_{i=1}^{L} h_i \hat{S}_i^z, \tag{S1}$$

where $J_z = 0.5$ and the on-site fields h_i are independent random variables uniformly distributed in $[-W, W]$. It is well-established that this model undergoes a phase transition from a thermal phase at weak disorder to a MBL phase at strong disorder.

Due to the $U(1)$ symmetry of $\hat{H}$, the total magnetization $\hat{S}_{\text{tot}}^z = \sum_{i=1}^{L} \hat{S}_i^z$ is a conserved quantity. Our analysis is performed via exact diagonalization within the largest symmetry sector, $\hat{S}_{\text{tot}}^z = 0$. To minimize finite-size effects and probe the bulk spectral properties, we sorted all eigenenergies within this sector in order and selected the middle one-third for our analysis. This selection process is consistent with the approach in Ref. [28].

The level spacing ratio for adjacent energy levels $\{E_n\}$ labeled in ascending order from smallest to largest is defined as:

$$r_n = \min\left(\frac{\delta_{n+1}}{\delta_n}, \frac{\delta_n}{\delta_{n+1}}\right), \tag{S2}$$

where $\delta_n = E_{n+1} - E_n$ represents the spacing between consecutive eigenenergies. We then construct histograms of the r_n distribution, $p(r)$ (see Fig. S1). In the thermalized phase, the distribution is expected to follow the Wigner-Dyson distribution, specifically the Gaussian Orthogonal Ensemble (GOE), while in the MBL phase, it should approach a Poisson distribution. The analytical expressions for $p(r)$ and the corresponding mean values of r (denoted by $\bar{r}$) for both Poisson and GOE statistics can be found in Ref. [112]. These theoretical predictions serve as benchmarks for identifying the phase of the system based on the observed level spacing statistics. Fig. S1 shows that $\hat{H}(W = 0.5)$ and $\hat{H}(W = 5.0)$ indeed lie in thermal phase and MBL phase, respectively.

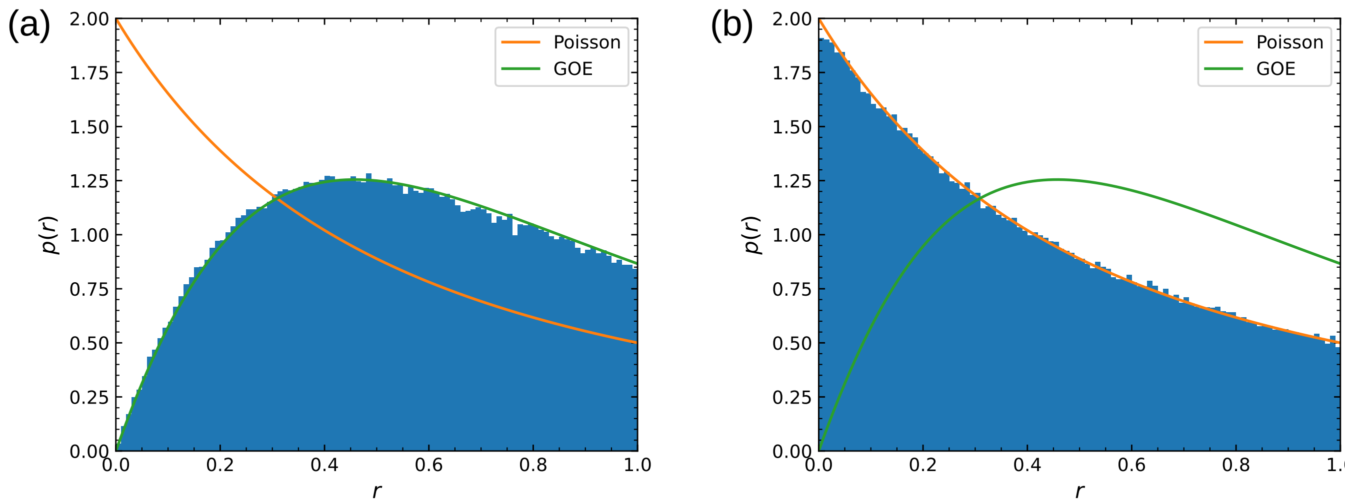

FIG. S1. Level spacing ratios distribution $p(r)$ of the Hamiltonian $\hat{H}$ (Eq. (S1)) for $L = 16$. For each panel, the distribution is computed from the middle one-third of the eigenenergies in the half-filling sector, with data compiled from 100 independent disorder realizations for the corresponding disorder strength W. Solid lines represent the theoretical predictions from RMT. (a) Thermal phase ($W = 0.5$). The distribution clearly follows the Wigner-Dyson form for the GOE. The numerically obtained average value of $\{r_n\}$ is about 0.531, is in excellent agreement with the GOE prediction $\bar{r} = 4 - 2\sqrt{3} \approx 0.536$ [112]. (b) MBL phase ($W = 5.0$). The distribution is well-described by Poisson statistics. The numerical average value of $\{r_n\}$ is about 0.388, closely matches the theoretical value for a Poisson distribution, $\bar{r} = 2\ln 2 - 1 \approx 0.386$ [112].

III. THE STATIONARY DISTRIBUTION OF THE BIPARTITIONS UNDER THE RANDOM SWAP CIRCUIT

Here, we provide an analytical proof that the Markov chain describing the evolution of bipartitions under the random SWAP circuit is ergodic and has a uniform stationary distribution. This Markov chain is time-homogeneous. Its state space consists of the $N = \binom{L}{L/2}/2$ distinct ways to partition the spin chain of even length L into two subsystems of size $L/2$.

We first establish the ergodicity of this Markov chain. For such a chain over a finite state space, a fundamental theorem states that ergodicity is equivalent to the chain being both irreducible and aperiodic. We now demonstrate these two properties.

The chain is irreducible because the set of adjacent SWAP gates generates the entire symmetric group of permutations. This means that any order of spins can be transformed into any other through a sequence of SWAP operations, ensuring that any bipartition is reachable from any other.

The chain is also aperiodic. For $L \geqslant 4$, there always exists at least one SWAP gate that acts on two spins within the same subsystem of a given bipartition (e.g., the standard half-chain bipartition). Such an operation leaves the bipartition unchanged, resulting in a non-zero self-transition probability, $P_{ii} > 0$. The existence of such a 1-step return path means that the set of all possible numbers of steps to return to state i contains the integer 1, which confirms that the chain is aperiodic.

Having established both irreducibility and aperiodicity, we conclude that this Markov chain is ergodic.

Next, we show that the stationary distribution w is uniform by invoking the detailed balance condition, $w_i P_{ij} = w_j P_{ji}$. For a uniform distribution, where w_i is constant for all states i, this condition simplifies to $P_{ij} = P_{ji}$. The transition probability from bipartition i to j is $P_{ij} = k_{ij}/(L-1)$, where k_{ij} is the number of SWAP gates that transform i to j. Since the SWAP gate is its own inverse, the exact same set of gates that transforms i to j also transforms j to i. Thus, $k_{ij} = k_{ji}$, which implies $P_{ij} = P_{ji}$. The detailed balance condition is therefore satisfied for a uniform distribution.

Finally, the ergodic theorem guarantees that an ergodic Markov chain converges to a unique stationary distribution irrespective of the initial distribution. We thus conclude that the random SWAP circuit drives the system towards a uniform stationary distribution over all possible equal-sized bipartitions.

IV. OTHER TYPES OF ENTANGLED INITIAL STATE AND THE CORRESPONDING RESULTS

To further probe the "build-move" framework and provide more targeted evidence for the "move-dominated" nature of MBL dynamics, we investigate the system's evolution starting from two distinct types of entangled states: "locally entangled" states and the eigenstates of the thermal Hamiltonian. In this section, the setups of Hamiltonian MBL and Floquet MBL dynamics are the same as those in the main text. Dashed lines in Fig. S2, Fig. S3, Fig. S4 and Fig. S5 still mark the Haar measure average HCEE in the half-filling sector.

A. Locally Entangled States

To create an ideal scenario for testing the "move" mechanism, we prepare initial states that possess significant entanglement within each half of the system but have strictly zero HCEE by construction. This provides a direct measure of the system's capacity to "move" entanglement.

These "locally entangled" states, denoted by $|\psi'(T)\rangle$, are prepared by evolving a sampled $|\psi_0\rangle$ for a duration T under a modified Hamiltonian, $\hat{H}_{\mathrm{local}}$, where the interaction across the central bond $(L/2, L/2+1)$ is explicitly removed:

$$\hat{H}_{\mathrm{local}} = \hat{H}(W=0.5) - \left(\hat{S}^x_{L/2}\hat{S}^x_{L/2+1} + \hat{S}^y_{L/2}\hat{S}^y_{L/2+1} + J_z\hat{S}^z_{L/2}\hat{S}^z_{L/2+1}\right). \tag{S3}$$

The definitions of $|\psi_0\rangle$ and $\hat{H}$ are the same as those in the main text. We still set $J_z = 0.5$ and $\hat{H}(W=0.5)$ is thermal as mentioned before. Consequently,

$$|\psi'(T)\rangle = \mathrm{e}^{-\mathrm{i}T\hat{H}_{\mathrm{local}}}|\psi_0\rangle. \tag{S4}$$

By design, the HCEE of $|\psi'(T)\rangle$ is zero, while the amount of entanglement within each subsystem serves as a "reservoir" that can be tuned by the preparation time T.

Fig. S2 shows the MBL evolution of the HCEE, starting from $|\psi'(T)\rangle$. As expected, the HCEE increases from 0, still exhibits logarithmic growth over time and eventually saturates at significantly increased but non-thermal values.

Fig. S3 plots the total HCEE growth. $\Delta S = S_{\mathrm{sat}} - S_{\mathrm{initial}} = S_{\mathrm{sat}}$ as $S_{\mathrm{initial}} = 0$. The values of T for the data points and the ways to determine the values of S_{sat} are the same as those for Fig. 1(d,e), both of which have been explained in detail in Sec. I.

The data presented in Fig. S2 and Fig. S3 are all averaged over 72 independent runs. Each run uses one sampled $|\psi_0\rangle$ and three sets of independently sampled disorders with strengths for corresponding Hamiltonian-based evolutions: one set of disorders for $\hat{H}_{\mathrm{local}}$ to prepare $|\psi'(T)\rangle$ and two sets of disorders for Hamiltonian MBL and Floquet MBL dynamics to quench $|\psi'(T)\rangle$.

Since the lines of 2 kinds of MBL dynamics are very close to the line of the random SWAP circuit for almost the whole range of T, Fig. S3 once again demonstrates that MBL is a kind of move-dominated dynamics for the growth of the HCEE.

B. Eigenstates of Thermal Hamiltonian

We now consider the MBL dynamics originating from the eigenstates of the thermal Hamiltonian $\hat{H}(W=0.5)$. These eigenstates span a wide range of HCEE values, providing a natural ensemble of initial states with varying

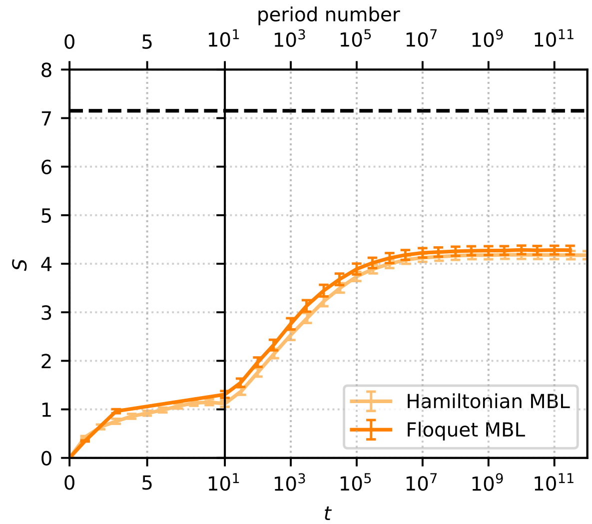

FIG. S2. Time evolution of HCEE S with initial state $|\psi'(T)\rangle$ for $L = 16$ and $T = 3.0$. The lower axis shows time t for the Hamiltonian MBL evolution, while the upper axis shows the period number for the Floquet MBL dynamics. To visualize the dynamics across multiple timescales, the horizontal axis uses a hybrid scale: it is linear for the initial evolution (t, period number < 10) and becomes logarithmic for long times.

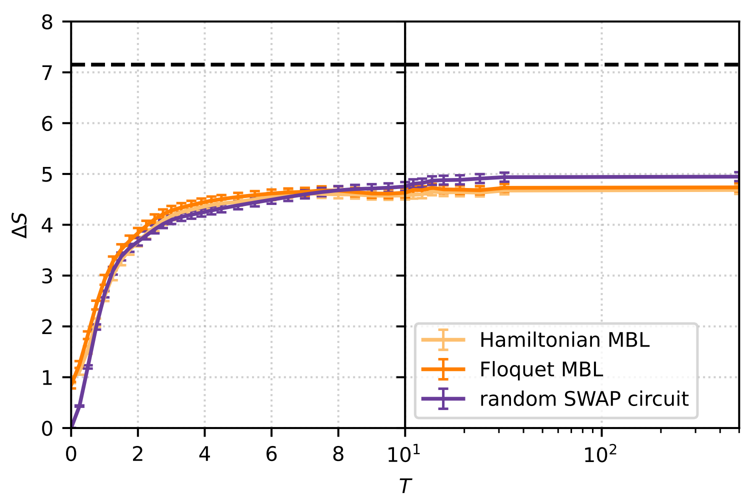

FIG. S3. The total growth of HCEE as a function of the preparation time T with initial state $|\psi'(T)\rangle$ for $L = 16$. In order to achieve good visualization of the data, the horizontal axis uses a hybrid scale: it is linear for the small T ($T < 10$) and becomes logarithmic for large T.

degrees of entanglement. Fig. S4 shows the results for the eigenstate whose energy ranks 29th from the lowest to the highest in the half-filling sector. The logarithmic growth over time and the non-thermal saturation value of HCEE have been maintained.

Fig. S5 plots the initial and saturated HCEEs for many eigenstates. The dimension of the half-filling sector for $L = 16$ is 12870. We sorted the eigenstates within it in ascending order of energy and selected the 1st, 2nd, 4th, 8th, 15th, 29th, 52nd, 87th, 142nd, 222nd, 337th, 494th, 704th, 978th, 1324th, 1750th, 2259th, 2855th, 3533rd, 4283rd, 5095th, 5950th, 6826th, 7700th, 8548th, 9348th, 10079th, 10727th, 11280th, 11737th, 12098th, 12371st, 12568th, 12701st, 12785th, 12833rd, 12857th, 12867th and 12870th ones to calculate the corresponding data. The ways to determine the values of S_{sat} are also the same as those for Fig. 1(d,e), which have been explained in detail in Sec. I.

The data presented in Fig. S4 and Fig. S5 are all averaged over 72 independent runs. Each run uses three sets of independently sampled disorders: one set of weak disorders for the thermal Hamiltonian to provide eigenstates and

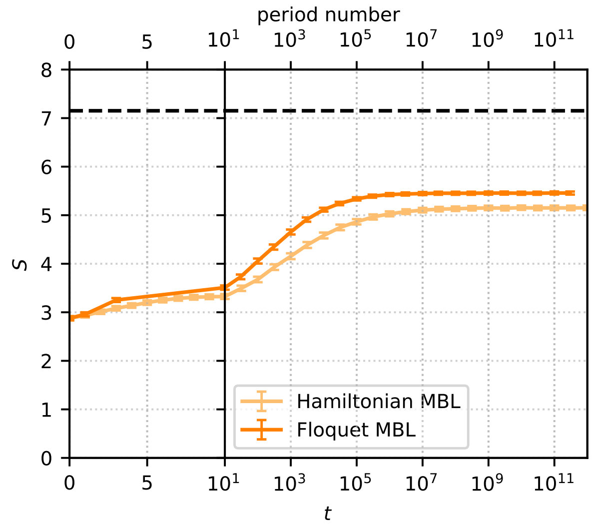

FIG. S4. Time evolution of HCEE S starting from the eigenstate whose energy ranks 29th from the lowest to the highest in the half-filling sector of $\hat{H}(W = 0.5)$ for $L = 16$. The lower axis shows time t for the Hamiltonian MBL evolution, while the upper axis shows the period number for the Floquet MBL dynamics. To visualize the dynamics across multiple timescales, the horizontal axis uses a hybrid scale: it is linear for the initial evolution (t, period number < 10) and becomes logarithmic for long times.

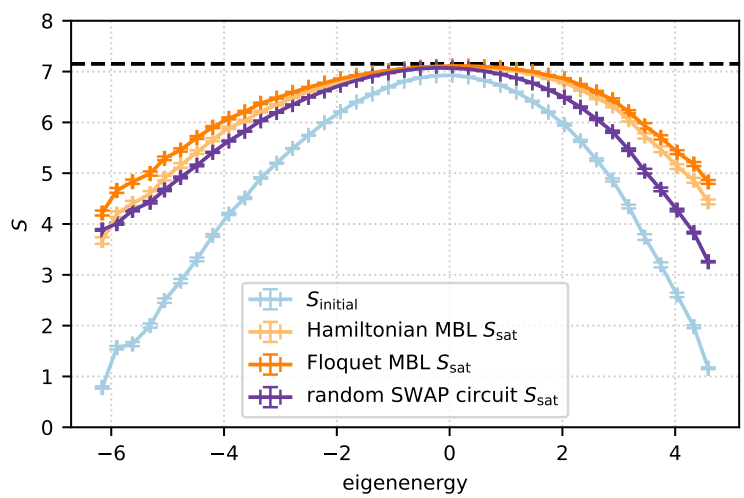

FIG. S5. The initial HCEE S_{initial} and saturated HCEE S_{sat} as a function of the eigenenergies. Initial states are the eigenstates in the half-filling sector of $\hat{H}(W = 0.5)$ for $L = 16$.

two sets of strong disorders for the quench dynamics of Hamiltonian MBL and Floquet MBL.

We can see that all four lines of S_{initial} and S_{sat} in Fig. S5 show a trend of first increasing and then decreasing. They reach their maximum values when eigenenergy is approximately equal to 0. By comparing the S_{sat} lines of two kinds of MBL dynamics to the S_{sat} line of the random SWAP circuit, we can also confirm that MBL is a kind of move-dominated dynamics for the growth of the HCEE.